An Experimental Kinetics Study of Isopropanol Pyrolysis and Oxidation behind Reflected Shock Waves

Sean P. Cooper *[ID]**, Claire M. Grégoire, Darryl J. Mohr** [ID]**, Olivier Mathieu, Sulaiman A. Alturaifi and Eric L. Petersen**

J. Mike Walker '66 Department of Mechanical Engineering, Texas A&M University, 3123 TAMU, College Station, TX 77843, USA; claire.gregoire@tamu.edu (C.M.G.); darrylapply1@tamu.edu (D.J.M.); olivier.mathieu@tamu.edu (O.M.); sulaiman.turaifi@tamu.edu (S.A.A.); epetersen@tamu.edu (E.L.P.)
* Correspondence: sean.cooper@tamu.edu

Abstract: Isopropanol has potential as a future bio-derived fuel and is a promising substitute for ethanol in gasoline blends. Even so, little has been done in terms of high-temperature chemical kinetic speciation studies of this molecule. To this end, experiments were conducted in a shock tube using simultaneous CO and H_2O laser absorption measurements. Water and CO formation during isopropanol pyrolysis was also examined at temperatures between 1127 and 2162 K at an average pressure of 1.42 atm. Species profiles were collected at temperatures between 1332 and 1728 K and at an average pressure of 1.26 atm for equivalence ratios of 0.5, 1.0, and 2.0 in highly diluted mixtures of 20% helium and 79.5% argon. Species profiles were also compared to four modern C3 alcohol mechanisms, including the impact of recent rate constant measurements. The Li et al. (2019) and Saggese et al. (2021) models both best predict CO and water production under pyrolysis conditions, while the AramcoMech 3.0 and Capriolo and Konnov models better predict the oxidation experimental profiles. Additionally, previous studies have collected ignition delay time (τ_{ign}) data for isopropanol but are limited to low pressures in highly dilute mixtures. Therefore, real fuel–air experiments were conducted in a heated shock tube with isopropanol for stoichiometric and lean conditions at 10 and 25 atm between 942 and 1428 K. Comparisons to previous experimental results highlight the need for real fuel–air experiments and proper interpretation of shock-tube data. The AramcoMech 3.0 model over predicts τ_{ign} values, while the Li et al. model severely under predicts τ_{ign}. The models by Capriolo and Konnov and Saggese et al. show good agreement with experimental τ_{ign} values. A sensitivity analysis using these two models highlights the underlying chemistry for isopropanol combustion at 25 atm. Additionally, modifying the Li et al. model with a recently measured reaction rate shows improvement in the model's ability to predict CO and water profiles during dilute oxidation. Finally, a regression analysis was performed to quantify τ_{ign} results from this study.

Keywords: shock tube; ignition delay time; chemical kinetics

1. Introduction

The transportation sector is overwhelmingly fueled by petroleum-derived liquid hydrocarbons, and many of these sources are supplemented using bio-derived oxygenates to limit environmental impacts and extend the life of petroleum reserves. While ethanol has been the common choice as a supplement for gasoline fuels for decades, the question remains whether there is a better alternative [1]. Investigating other alternatives requires not only coupling physical and combustion characteristics but also jointly optimizing the fuel itself and its ability to efficiently produce energy within internal combustion engines (ICEs). The recent Co-Optimization of Fuels and Engines project by the Department of Energy has given many insights into possible bio-derived blendstocks for gasoline specifically [2–4]. From this program, Gaspar et al. published a list of bio-derived fuels highlighting ten fuels showing the most potential as gasoline additives [4]. Of these 10, 6

were chosen as having the fewest barriers to adoption (stability, compatibly, engine impact, etc.), and isopropanol was among these 6. Not only is isopropanol chemistry important to future transport sector applications, but interestingly its importance to the chemical kinetics of organophosphorus compounds has recently been shown [5]. Additionally, isopropanol kinetics have been shown to be a major aspect in liquid monopropellant combustion [6].

Previous studies have made efforts to develop experimental data for isopropanol combustion using flow reactors, flame speed measurements, and shock tubes. The first chemical kinetics study was presented by Smith and Gordon in 1956 in a diffusion flame [7]. Norton and Dryer more recently recorded species profiles of isopropanol (among many other alcohols) within a flow reactor [8]. Sinha and Thomson and Frassoldati et al. utilized counter-flow diffusion flames to collect species profiles [9,10]. Esarte et al. used a flow reactor to study isopropanol pyrolysis and oxidation in acetylene mixtures [11]. Li et al. also utilized a flow reactor to study speciation of isopropanol combustion for pressures between 0.04 and 1 atm with 97% argon dilution, but they also experimentally determined laminar burning velocities (LBVs) using a constant-volume vessel at pressures up to 10 atm [12]. Premixed isopropanol flames have been studied by Li et al. and Kasper et al. at considerably lower pressure (<0.1 atm) [13,14]. Togbe et al. performed the first isopropanol experiments in jet-stirred reactors (JSRs) as well as collected LBVs at pressures up to 10 atm in validating the model they presented [15].

Johnson et al. presented the first ignition delay time (τ_{ign}) measurements for isopropanol for temperatures between 1350 and 2000 K at 1 atm in mixtures diluted in at least 97.25% argon [16]. Akih-Kumgeh and Bergthorson also presented τ_{ign} data but at pressures up to 12 atm in an 89% argon-diluted mixture [17]. Man et al. presented the highest-pressure τ_{ign} data at 16 atm, however they were under highly diluted conditions [18]. Most recently, Jouzdani et al. measured ignition delay times and CO time histories in a shock tube for isopropanol [19]. The CO laser absorption measurements were conducted in dilute mixtures at 3 atm, while τ_{ign} values were measured mainly in dilute mixtures. However, a set of experiments was conducted with "airgon" (79% Ar, 21% O_2 oxidizer mixture) for stoichiometric conditions at 12 atm. Note that higher pressures have been investigated in rapid compression machines (RCMs) for intermediate temperatures [20]. In summary, very few data are available above 10 atm, and even fewer are available for real fuel–air conditions. Additional data are required for better prediction and understanding of isopropanol combustion for use in ICEs.

To this end, experiments were conducted to collect τ_{ign} data at real fuel–air and higher pressures by the authors. Comparisons are made with the Jouzdani et al., where agreement is seen for lower temperatures, but disagreement at higher temperatures is used as a point of discussion. While Jouzdani et al. did conduct CO laser absorption measurements at 3 atm, these results were limited to isopropanol pyrolysis, and therefore additional CO measurements were made in the present study at near-atmospheric pressure for isopropanol pyrolysis and oxidation. Additionally, novel H_2O measurements during isopropanol oxidation near atmospheric pressure were taken to further model predictions of target molecules. In particular, model predictions using a recent reaction rate measurement made by the authors show good improvement, although not as dramatically as those made for the smaller ethanol molecule [21–23]. It should also be noted that another measurement of this reaction rate was made recently by Mertens and Manion in a single-pulse shock tube, but for a lower temperature range [24].

Further efforts have also been made in developing chemical kinetics models to characterize and predict isopropanol combustion. Johnson et al., besides presenting the first τ_{ign} data, also presented the first chemical kinetic model aimed at combustion of propanol isomers [16]. Man et al. then used Johnson et al. (among others) as the basis for their model, making improvements on the overall predictions of τ_{ign} for dilute mixtures and pressures up to 16 atm, as well as on speciation in flow reactors and flame speed measurements. Frassoldati et al. produced the second model using speciation measurements in a counter-flow diffusion flame at 1 atm to validate their predictions; this would form the basis of

the propanol submechanism for the CRECK modeling group [10]. Additional modeling efforts were made by Veloo and Egolfopoulos using LBV measurements at 1 atm for model validation [25]. A comprehensive study was conducted by Sarathy et al., discussing the chemistry of alcohols in general, including propanol isomers, providing guidance on alcohol combustion modeling and the state of current experiments [26]. Many of the reactions presented by Sarathy et al. were utilized within the recent AramcoMech 3.0 model [27]. Liu et al. also presented a model for several alcohols using the available literature [28]. More recently, the Li et al. model was presented with new flow reactor and LBV measurements. This model would become the basis for a recent reaction rate kinetics measurement [21]. Finally, the most recent models by Capriolo-Konnov and Saggese et al. represent the most up-to-date and comprehensive models based on the literature available [29,30]. For the purposes of this study, the latest four models (AramcoMech 3.0, Li et al., Capriolo Konnov, and Saggese et al.) were used for comparison and analysis.

Herein, the shock tube and laser diagnostics are first described, and definitions for ignition delay time as well as a description of the mixtures used are provided. Results and model predictions from the laser diagnostics are next described beginning with the pyrolysis results for water and CO followed by the oxidation results. Then the τ_{ign} values and model predictions are presented with a sensitivity analysis for τ_{ign} by the two models that best predict τ_{ign}. The discussion section then addresses improvements to model predictions using new reaction rates and the effect helium addition has on the dilute mixtures investigated.

2. Experimental Methods

For collecting multiple, different datasets and types in this study, both a low-pressure and a high-pressure shock tube were used for the laser absorption and ignition delay time experiments, respectively. The facilities and their optical diagnostics are further discussed in the following subsections.

2.1. Shock Tubes

The Aerospace Shock Tube (AST) facility at Texas A&M University was utilized to produce the lower-pressure conditions needed for the laser absorption experiments. This facility has a driven inner diameter and length of 16.2 cm and 7.88 m, respectively. The shock tube is pressure driven and utilizes single, polycarbonate diaphragms to initiate shock propagation. For the conditions investigated herein, 0.25-mm-thick diaphragms were used to generate pressures around 1.4 atm behind the reflected shock. A downstream, cross-shaped cutting blade was used to facilitate ideal and repeatable diaphragm rupture. To measure the incident-shock velocity, five piezoelectric pressure transducers (PCB P113A22) were employed to detect shock passage over the last 2 m of the shock tube. This configuration allows a linear fit through the measured velocities to be extrapolated to estimate the incident-shock velocity once it reaches the endwall, 1.6 cm downstream from the last (sidewall) pressure transducer. From here, the reflected-shock pressure and temperature can be calculated to within uncertainties of $\pm1\%$ and $\pm0.8\%$, respectively [31]. Using helium as the driver gas allowed for test times up to 3 ms for the conditions investigated. Four sapphire optical window ports at the sidewall location, 1.6 cm upstream from the endwall, were used to allow simultaneous CO and water laser absorption measurements. Additionally, an RTV silicone-shielded pressure transducer (PCB P113A22) was located at the same axial position to monitor pressure during the experiment. It has been demonstrated previously that the conditions investigated herein allow for minimal non-ideal effects due to boundary-layer growth in the AST, particularly due to the use of mainly argon as a driven gas and the relatively low pressures [32,33]. Both shock tubes were evacuated to 10^{-5} Torr prior to adding the test mixture to ensure mixture purity using a combination of a rotary vane pump (Agilent DS 602 and DS 402) and a turbomolecular pump (Agilent Turbo V1001 Navigator). Further details on the AST facility can be found elsewhere [34].

For the real fuel–air ignition delay time measurements, the heated high-pressure shock tube (HPST) facility at Texas A&M University was utilized. The shock tube's driven section has an inner diameter of 15.24 cm and is 5.03 m in length. The incident shock velocity measurement is nearly identical to that of the AST, with four pressure transducers (PCB 113B22) being utilized over the last 1.44 m of the shock tube to produce three incident-shock velocity measurements for estimating the shock velocity at the endwall location. With this setup, similar uncertainties in pressure and temperature are achieved. The uncertainty in temperature translates to ±20% uncertainty in ignition delay time, which has recently been shown by Zander et al. to be fairly conservative for these conditions [35]. To generate 10-atm, post-reflected shock pressures (P_5), 2-mm-thick polycarbonate diaphragms were used, utilizing a similar downstream cutting scheme as in the AST. For P_5 pressures above 10 atm, aluminum diaphragms (also 2 mm thick) were used with a pre-scored cross pattern for similar reliability and ideal rupture as seen with the polycarbonate diaphragms. Again, helium was used as the driver gas, which allowed for a maximum test time of 2.5 ms. Even so, boundary-layer growth within shock tubes is exacerbated when dealing with driven gases other than argon [36]. However, due to the large inner diameter of the HPST, non-ideal effects are minimized, particularly the post-reflected-shock pressure rise (dP^*/dt) [37]. Further details on the heating system and HPST have been provided previously [38,39].

Mixtures for the highly dilute experiments (99.25–99.5% argon and helium) were made manometrically using a 22.2 L mixing tank. Prior to mixing, the tank was evacuated to a pressure below 10^{-5} Torr using the turbomolecular pump. A vial was filled with isopropanol and connected to the gas handling manifold, which was then degassed several times to ensure that only isopropanol existed within the vial. Mixtures were measured using two capacitance manometers (MKS Baratrons with 0–10 Torr and 0–1000 Torr ranges) and a pressure transducer (Setra GCT-225, 0–17 bar range) for the AST's mixing tank. To ensure isopropanol did not condense, the partial pressure was kept below 10% of its vapor pressure (~32.8 Torr at 20 °C). The same was true for the HPST experiments; however this required the shock tube to be heated to 60 °C and for mixtures to be made directly into the shock-tube driven section for each experiment. Similar to the dilute mixtures, isopropanol was added to the driven section using a degassed vial attached to the gas handling manifold. Once the desired partial pressure of isopropanol was achieved, the driven section was quickly filled with a synthetic air mixture to encourage turbulent mixing. The mixture was then allowed to further mix for at least 20 min prior to diaphragm rupture. This process has been successfully demonstrated previously with fuels with much lower vapor pressures (Jet-A, RP-1, and diesel) [38]. A compilation of the mixtures used and the conditions investigated in this study is shown in Table 1.

Table 1. Summary of the mixtures and conditions investigated herein. Note, pressures are listed as the average and depict the range of test-to-test variation not the uncertainty.

	Mixture Composition (% mol)				Conditions		
Mix	iC$_3$H$_7$OH	O$_2$	Diluent	φ	P$_5$ (atm)	T$_5$ (K)	Measurement
1	0.75%	N/A	99.25% Ar	Inf.	1.42 ± 0.10	1127–2162	Water Abs.
2	0.75%	N/A	20.07% He + 79.18% Ar	Inf	1.29 ± 0.09	1173–1669	Water and CO Abs.
3	0.05%	0.45%	20.11% He + 79.39% Ar	0.5	1.28 ± 0.07	1341–1519	
4	0.09%	0.41%	20.08% He + 79.42% Ar	1.0	1.25 ± 0.12	1416–1646	
5	0.09088%	0.4112%	99.7492% Ar	1.0	1.36 ± 0.15	1419–2073	
6	0.1540%	0.3444%	20.0456% He + 79.456% Ar	2.0	1.22 ± 0.06	1470–1728	
7	2.281%	20.529%	77.19% N$_2$	0.5	10.2 ± 0.8	1068–1410	OH* τ$_{ign}$
					24.5 ± 3.4	995–1311	
8	4.46%	20.07%	75.47% N$_2$	1.0	10.2 ± 1.2	1022–1428	
					26.5 ± 3.2	942–1186	

2.2. Optical Diagnostics

Two laser absorption diagnostics were utilized to simultaneously measure water and CO production during the same experiment via multiple window ports allowing access to the sidewall location, 1.6 cm downstream from the endwall of the AST. Only a brief discussion on these diagnostics is provided here, but more detailed information on the water and CO diagnostics has been described in previous studies [40–43].

The water diagnostic utilized a Toptica Photonics DL100L tunable diode laser set to 1388.140 nm. This wavelength allows access to the $5_{5,1} \leftarrow 5_{5,0}$ transition in the fundamental $\nu_1 + \nu_3$ band. A Burleigh WA-1000 wavemeter was used to monitor the wavelength. Two detectors (Newport 2317NF InGaAs) fitted with a 1388 nm (10 nm full width at half maximum (FWHM)) bandpass optical filters allowed for the measurement of incident and transmitted light intensities (I_0 and I, respectively). The beam path was contained within a N_2-purged environment to reduce laser attenuation due to air humidity.

A quantum cascade laser with a 1.5 MHz line width allowed access to the R(12) transitions $1 \leftarrow 0$ band of CO at 4566.17 nm. A CO/Ar mixture contained in a separate cell was introduced into the beam's path to center the laser on the CO transition line. Detectors (InSb) fitted with bandpass filters centered at 4500 nm with 500 nm FWHM allowed for collection of incident and transmitted light intensities with <0.3% broadband emission levels compared to the absorption signal. It should be noted that the procedure described by Mulvihill et al. was used to subtract the minor CO_2 absorbing species to extract the final CO time histories [44].

Note, for both diagnostics, experiments were conducted with the lasers off where no broadband emission was observed. Additionally, off-line experiments were performed and showed no interfering species during isopropanol combustion or pyrolysis. The H_2O fixed-wavelength diagnostic utilized diode temperature and current controllers (Toptica Photonics models DTC 110 and DCC 110, respectively) to permit stable and consistent laser operation. For the CO diagnostic, similar controllers were used, and frequent verifications were performed to ensure the laser was centered on the transition line. In this case, checks were made prior to each experiment. Temperature predictions made by the Li et al. model were used to account for temperature change during combustion and pyrolysis for both laser diagnostics. The mixtures were chosen to keep the temperature change below 150 K. Finally, previous studies estimated the uncertainties of the water and CO measurements at around 5.6% and 3.8%, respectively [43].

Ignition delay time measurements were taken using an OH* chemiluminescence (near 307 nm) diagnostic at the sidewall and endwall locations. Two photomultiplier tubes (Hamamatsu 1P21) equipped with UV filters (307 nm center, 10 nm FWHM) were used to gather OH* time histories in the real fuel–air mixtures. Ignition delay time was then defined by the difference between reflected-shock arrival and the linear extrapolation to zero emission of the steepest increase of OH* emission at either the sidewall or endwall locations. Pressure rise due to combustion can also be used to define the time ignition begins. For real fuel–air experiments (i.e., undiluted), time zero (reflected-shock arrival) is always defined by the time of shock reflection at the endwall [45]. Figure 1 defines τ_{ign} using a representative experiment from this study. Note also that simultaneous sidewall and endwall pressure and OH* emission were monitored during each experiment to ensure homogeneous combustion [22].

2.3. Modeling

To assess modern chemical kinetic mechanism predictions of isopropanol oxidation and pyrolysis for dilute and real fuel–air conditions, the closed homogeneous reactor in Chemkin 19.1 from Ansys was utilized [46]. Therein, the "Constrain Volume and Solve Energy Equation" assumption was used. As discussed, $dP*/dt$ was minimal and, therefore, was not included in modeling the experimental conditions.
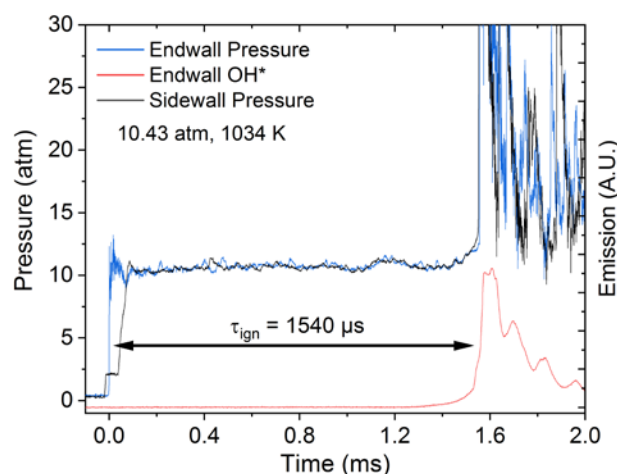
Figure 1. Representative pressure and OH* emission time histories for an experiment at stoichiometric conditions for isopropanol combustion in real fuel–air. Here, τ_{ign} is defined as the difference between shock reflection at the endwall and the steepest initial rise in OH* signal at the endwall.

Previous work by the authors investigated isopropanol pyrolysis kinetics using the Li et al. model and AramcoMech 3.0 but also included models by Man et al., Togbe et al., and one from the CRECK modeling group [15,18,47]. Herein, only the most recent models were chosen for comparison purposes both for simplicity and with the knowledge that the older models by Man et al., Togbe et al., and CRECK performed poorly previously, and improvements have since been made [21]. It should be noted that the Saggese et al. model does not include helium as a species. Therefore, when modeling mixtures that included helium with the Saggese et al. model, the percentage of the mixture that was helium was assumed as argon (i.e., the real mixture had 20% He and 79.25% Ar and the modeled mixture was simply 99.25% Ar). Further details of the four chemical kinetics models used for comparison in this study are given in Table 2.

Table 2. Characteristics of the four chemical kinetic models used for comparison with experiments.

Model	# Species	# Reactions	Year
AramcoMech 3.0	581	3037	2018
Li et al.	156	1394	2019
Capriolo and Konnov	161	1787	2020
Saggese et al.	371	2318	2020

3. Results

Several datasets were taken for this study to investigate isopropanol chemical kinetics in multiple unexplored areas to better establish our understanding of the combustion kinetics of isopropanol. These datasets include CO and water laser absorption measurements during isopropanol pyrolysis and oxidation near atmospheric pressure in mixtures highly diluted in argon. Additionally, ignition delay time measurements were taken under "real" fuel–air conditions at elevated pressures.

3.1. Pyrolysis

Experiments conducted under pyrolysis conditions around 1.4 atm for three temperatures are shown in Figure 2. Note, the mixtures used for the pyrolysis H_2O time histories did not contain helium and consisted only of 0.75% isopropanol and argon (Mix 1 in Table 1). Note, for all the laser absorption experiments, spikes in the laser signal were seen before time zero. These spikes do not indicate sudden water or CO production, but

rather are a result of the schlieren effect caused by the changing density across the incident and reflected shock.
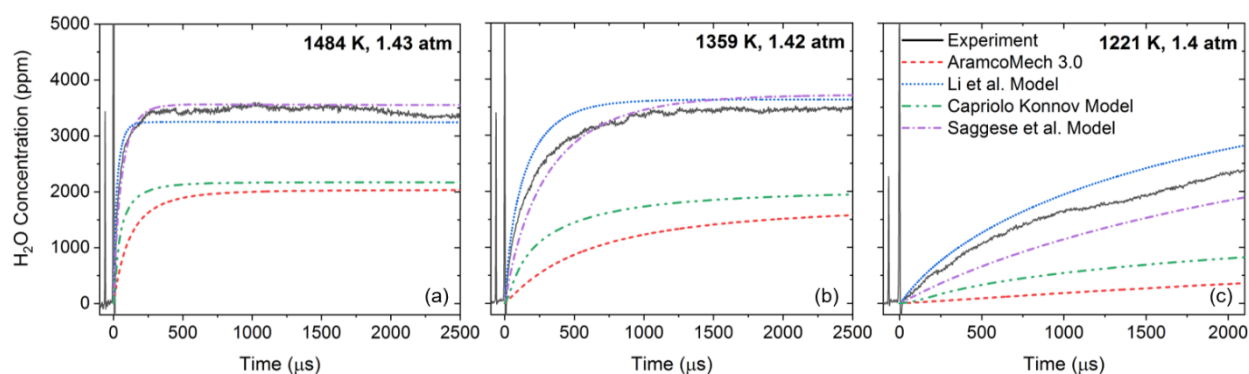

Figure 2. Experimental H_2O time histories isopropanol pyrolysis (Mix 1) for three temperatures ((**a**) 1484 K, (**b**) 1359 K, and (**c**) 1221 K) near 1.4 atm compared to four model predictions.

Consistent under prediction was made by the AramcoMech 3.0 and the Capriolo and Konnov model, while overall good agreement was seen for the Li et al. and Saggese et al. models. Previous sensitivity analyses showed that the production of water during isopropanol pyrolysis under these conditions is mainly controlled by the unimolecular dehydration of isopropanol via (R1) [21].

$$iC_3H_7OH \rightleftharpoons H_2O + C_3H_6 \tag{R1}$$

Therefore, model prediction of water production at these conditions is highly dependent on a model's choice of reaction rate for (R1). To examine this in further detail, Table 3 shows the reaction rates for (R1) utilized by each of the four kinetics mechanisms.

Table 3. Reaction rates for (R1) from each of the four kinetics mechanisms investigated herein.

Model	A (s^{-1})	n	E$_a$ (cal/mol)
Li et al.	1.87×10^{38}	-6.8	81,200
AramcoMech 3.0	5.00×10^{13}	0	68,000
Capriolo and Konnov	5.00×10^{13}	0	68,000
Saggese et al.	8.52×10^6	2.12	60,935

Note, Li et al. uses a modified unimolecular dehydration reaction for tert-butanol from Jin et al., who used a variation on the unimolecular dehydration reaction of n-butanol calculated using Rice–Ramsperger–Kassel–Marcus (RRKM) theory by Cai et al. [48,49]. That is, the reaction rate used by Li et al. is twice removed from a previous theoretical calculation for a different molecule. Capriolo and Konnov and AramcoMech 3.0 both adapted the dehydration reaction for isobutanol presented by Sarathy et al., who adapted it from the dehydration reaction of 2,3-dimethylbutan-2-ol as described by Tsang [50,51]. Meaning again that a reaction rate for a different molecule is nearly estimated as being close to that of the actual rate for (R1). However, Saggese et al. utilizes the experimental reaction rate measured by Heyne et al., who reported three reaction rate measurements at 976, 978, and 999 K at a pressure of 12.5 atm [52]. In other words, Saggese et al. is the only model to utilize a reaction rate for (R1) that was experimentally determined. In fact, Saggese et al. uses the only reaction rate determined for and with isopropanol. Even so, the reaction rate from Heyne et al. is over a very narrow temperature range and would over predict the reaction rate if extrapolated to higher temperatures [21]. The implications of (R1) rate coefficient choice are shown by the severe under prediction by the Capriolo and

Konnov and AramcoMech 3.0 models. Additional comparisons were later investigated herein to examine the use of recently measured reaction rates for (R1), particularly in its assistance in model predictions during oxidation.

Representative CO time histories for experiments conducted using 0.75% isopropanol mixtures diluted in helium and argon (Mix 2 in Table 1) are shown in Figure 3. Model predictions for the experiments measuring CO production during isopropanol pyrolysis showed similar results to the water measurements, where the Li et al. and Saggese et al. models performed the best in terms of shape and value prediction. Particularly good agreement was seen for the intermediate-temperature case for Li et al. (Figure 2b), although it did over predict CO formation for the high- and low-temperature cases (Figure 2a,b, respectively) where the Saggese et al. model performed the best. AramcoMech 3.0 and Capriolo and Konnov both predicted significantly different behavior than that shown by experiment. Particularly poor prediction in shape and value was seen for the intermediate-temperature profile (Figure 2b). However, AramcoMech 3.0 and Capriolo and Konnov predicted the low-temperature case well in terms of shape, although still under predicting the experimental values. Over prediction at higher temperatures was seen for all models. However, while Saggese et al. significantly under predicted CO values for nearly all conditions, it best predicted the high-temperature results. Overall, poor model predictions were seen for CO during isopropanol pyrolysis, with widely varying predictions made by the models.
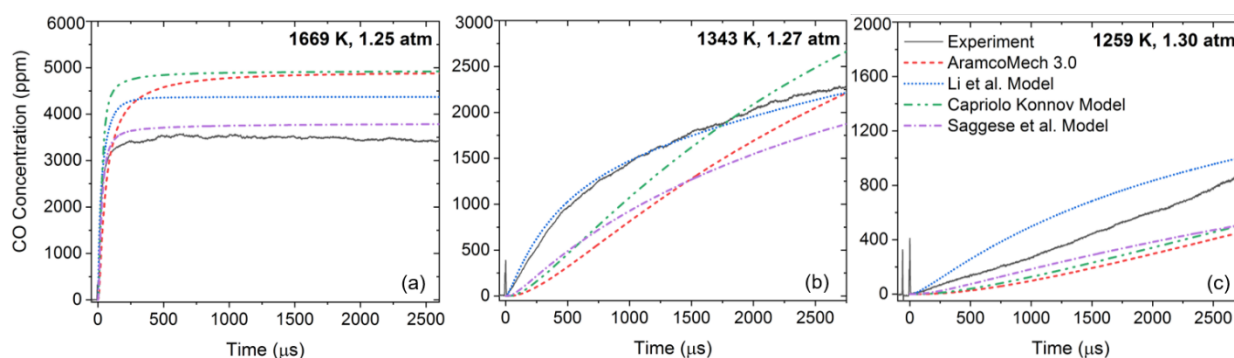

Figure 3. CO time-history results for (**a**) high-, (**b**) intermediate-, and (**c**) low-temperature cases near 1.3 atm in Mix 2 from Table 1. Predictions made by the four kinetics models are also shown.

3.2. Oxidation

Isopropanol oxidation was examined under dilute conditions (20% He, 79.5% Ar) for φ = 0.5, 1.0, and 2.0 (Mixtures 3, 4, and 6 in Table 1). Figures 4 and 5 depict representative H_2O and CO species time histories, respectively. Examples for two temperature cases for each of the stoichiometric ((a) and (b)) and fuel-rich ((c) and (d)) mixtures are shown.

Water formation during isopropanol pyrolysis is characterized by two main features, an initial production from the endothermic decomposition of isopropanol (mainly via (1)) followed by the formation of water through exothermic oxidation. Note, the noise in the oxidation results was higher than that of the pyrolysis experiments due to the diagnostic's cooling element's sensitivity to fluctuations in room temperature. Additionally, there is a spike around 2 ms in Figure 4d due to a diaphragm fragment, and it is not a jump in water production. Overall, the models by Li et al. and Saggese et al. predicted the initial water production well. Conversely, predictions by AramcoMech 3.0 and Capriolo and Konnov under predicted this initial production. However, AramcoMech 3.0 and Capriolo and Konnov performed the best at predicting the timing and shape of the secondary increase in water production amongst the four models. Naturally, at higher temperatures, all models performed well at predicting the shape and timing of water production, although disagreement was seen for plateau values in fuel-rich mixtures. Particularly, in Figure 4c, Li et al. and Saggese et al. show a much more dramatic decrease in water after peak

production than that seen in the experiment. Here, Capriolo and Konnov was the only model that predicted the behavior of the final plateau well.
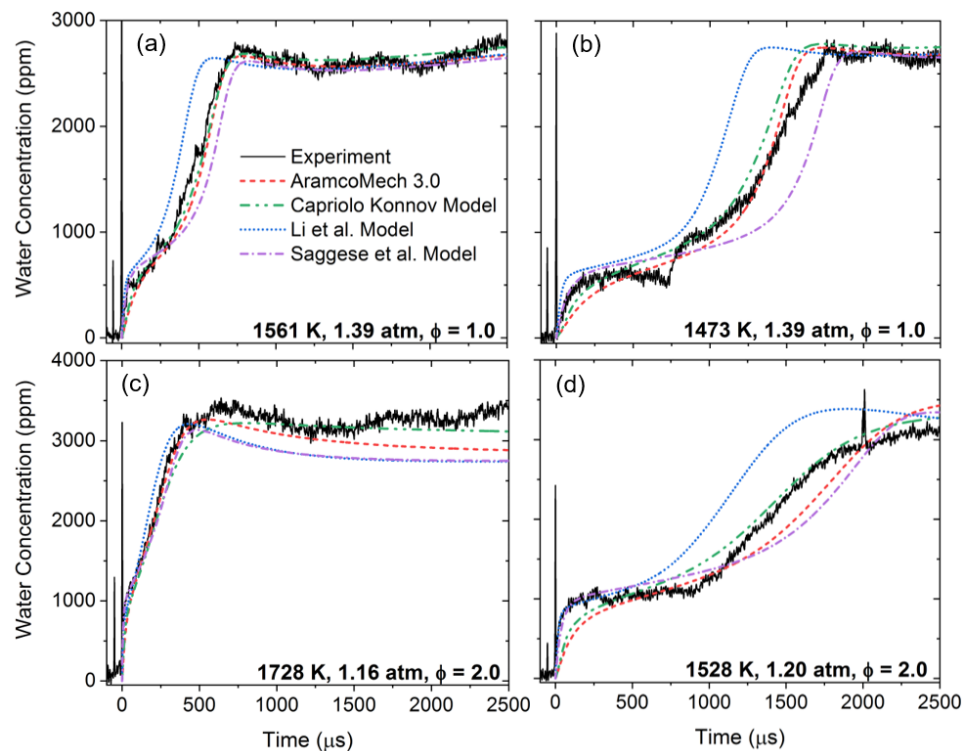

Figure 4. Water time-history results for isopropanol oxidation at φ = 1.0 (**a**,**b**) and 2.0 (**c**,**d**) around 1.3 atm for high- (**a**,**c**), and low-temperature (**b**,**d**) cases. Predictions by the four chemical kinetic models are also shown for comparison.
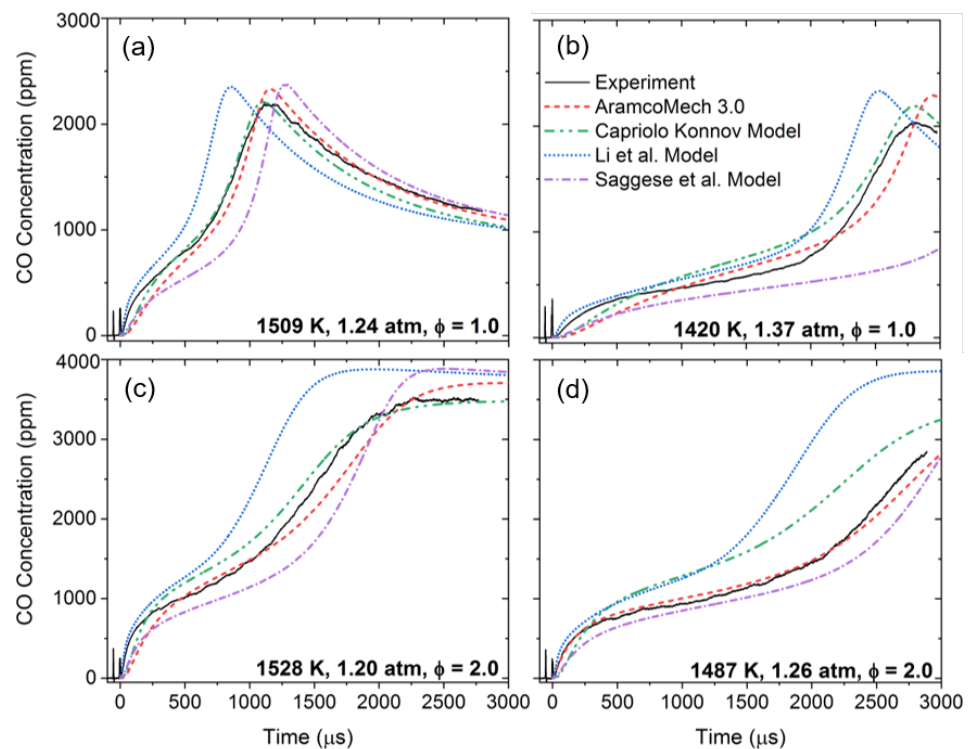

Figure 5. CO time history results for isopropanol oxidation at φ = 1.0 (**a**,**b**) and 2.0 (**c**,**d**) around 1.3 atm for intermediate- (**a**,**c**) and low-temperature (**b**,**d**) cases.

Figure 5 shows representative results for measurements taken with the CO laser diagnostic. For all conditions, Li et al. predicted CO formation much earlier than observed in the experiment, by about 1 ms, while Saggese et al. greatly under predicted CO formation values and timing. AramcoMech 3.0 and Capriolo and Konnov showed the best agreement with the experimental CO profiles. However, as expected from observations from the pyrolysis experiments, AramcoMech 3.0, Capriolo and Konnov, and Saggese et al. under predicted the initial CO formation, while Li et al. predicted this initial rise well, with some over predictions for lower temperatures.

3.3. Ignition Delay Time

As defined earlier, τ_{ign} data were collected using the HPST for real fuel–air conditions at elevated pressures. Results at 10 atm were similar to those obtained by Jouzdani et al., who collected a set of τ_{ign} data at 12 atm for stoichiometric conditions (Mix 7 in Table 1) [19]. A comparison between the data collected herein and those by Jouzdani et al. is shown in Figure 6.
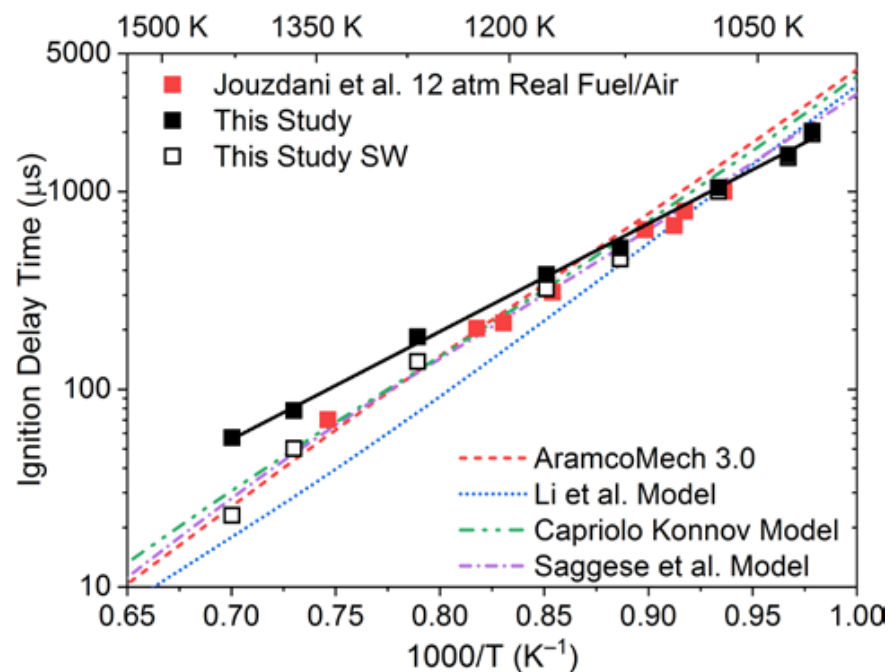

Figure 6. Comparison of stoichiometric, real fuel–air data from this study at 10 atm and those taken by Jouzdani et al. at 12 atm. Predictions made by the four models are also shown.

Good agreement was seen between data from this study and Jouzdani et al. for lower-temperature results. However, the results began to deviate as temperature increased. This deviation can be attributed to Jouzdani et al.'s use of sidewall measurements to define τ_{ign} as opposed to the endwall measurements used in this study. It is well known that sidewall τ_{ign} made in non-dilute mixtures will result in noticeably shorter τ_{ign} measurements for times less than about 100 µs; in fact, the example is strikingly similar to endwall and sidewall comparisons made previously [45]. As sidewall measurements were also taken during the present experiments to ensure homogeneous ignition, these diagnostics allowed for the measurement of sidewall τ_{ign} data, and these results are also shown in Figure 6 [22]. Unsurprisingly, sidewall τ_{ign} values from the present study showed good agreement with those presented by Jouzdani et al. when analyzed in the same way. Additionally, good agreement was also seen for the AramcoMech 3.0, Capriolo and Konnov, and Saggese et al. models with the sidewall τ_{ign} data. This good agreement indicates that they have been tuned to the data with an artificially higher activation energy. The actual slope (and ignition activation energy) should look more like the solid black line in Figure 6.

A comparison between $\varphi = 0.5$ and 1.0 (Mixtures 7 and 8 in Table 1, respectively) results from this study is shown in Figure 7. Model predictions for the fuel-lean case are also shown. Interestingly, the models, particularly the Saggese et al. and Capriolo and Konnov models (Figure 7a), did a good job of predicting the data for the fuel-lean case, even in terms of the activation energy, which all models over predicted for the stoichiometric case, as shown in Figure 7. Over prediction in excess of 68% was seen by AramcoMech 3.0 for low temperatures. Severe under prediction by the Li et al. model was seen for high temperatures, with τ_{ign} values less than half those of the experimental values. This result is similar to that seen in the laser absorption experiments, where the Li et al. model generally predicted water and CO formation earlier than that seen by experiment. Additionally, a coalescence of results was seen between the two cases at high temperatures. This phenomenon was also predicted by the Capriolo and Konnov and Saggese et al. models, but the convergence was seen at slightly higher temperatures, which may also be related to the overestimation of the activation energy from the artificially accelerated sidewall τ_{ign} measurements.
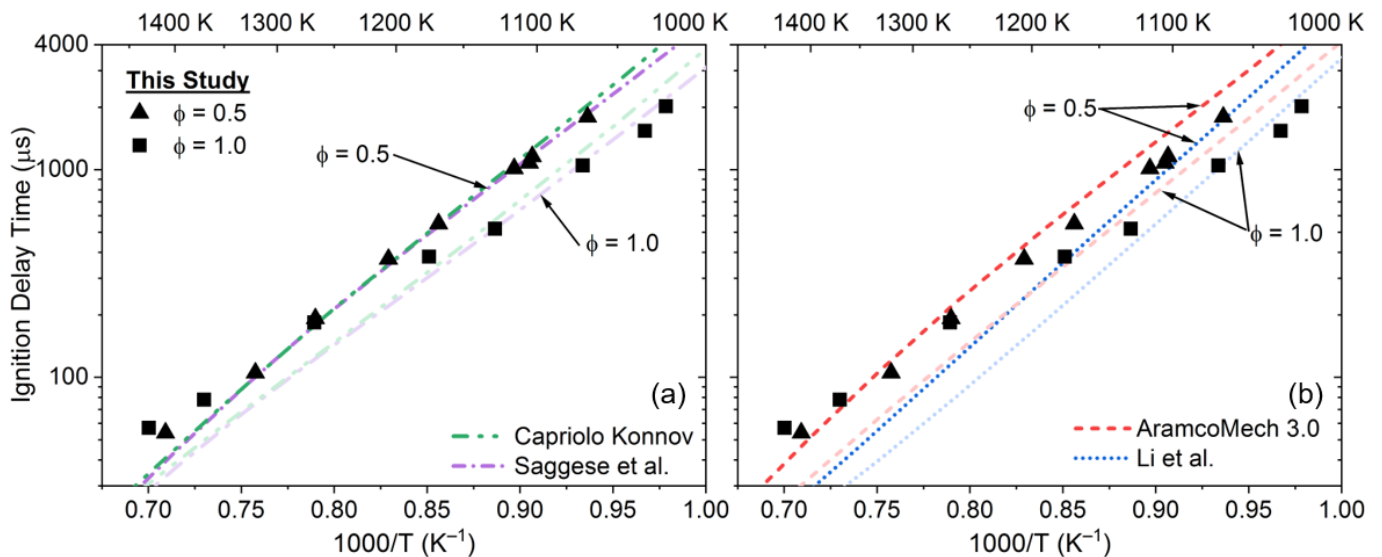

Figure 7. Ignition delay time results for the fuel-lean and stoichiometric cases at 10 atm. Model predictions are also shown for (**a**) Capriolo and Konnov and Saggese et al. and (**b**) AramcoMech 3.0 and Li et al.

Additional τ_{ign} experiments were conducted at 25 atm, and the results are compared to those at 10 atm in Figure 8. As the Capriolo and Konnov and the Saggese et al. models performed the best at 10 atm, their model predictions for the 25 atm data are also shown in Figure 8. Similar to the 10 atm predictions, Saggese et al. predicted the best ignition delay time results among the four models.

Therefore, the model by Capriolo and Konnov showed the best agreement across all experiments studied herein (CO and water time histories and real fuel–air ignition delay times). However, the model did not perform well for the more fundamental pyrolysis experiments. Saggese et al. did particularly well for the pyrolysis experiments and also for the global τ_{ign} measurements but fell short in its CO and water time history oxidation predictions. The AramcoMech 3.0 model predicted CO and water production well for the oxidation experiments but performed poorly for the pyrolysis and τ_{ign} experiments. Finally, the Li et al. model only performed well for the pyrolysis experiments.
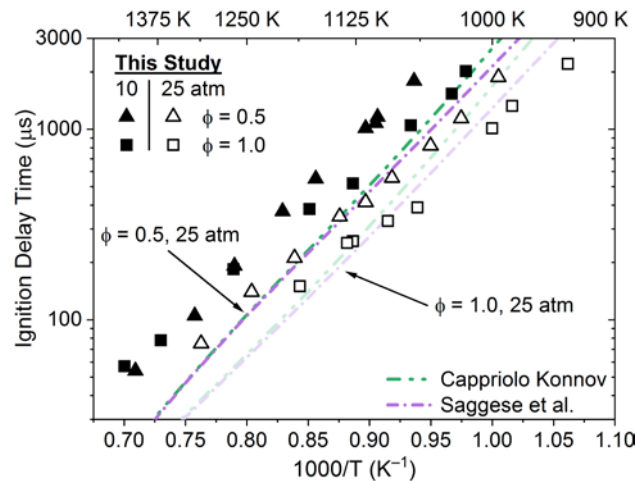
Figure 8. Comparison of all ignition delay time data collected herein. Model comparisons by the Capriolo and Konnov and the Saggese et al. models are shown for the 25-atm experiments.

Figure 9 shows the top 10 reactions that τ_{ign} was most sensitive to according to the Capriolo and Konnov and Saggese et al. models. Notably, the most sensitive reaction for Saggese et al. (and second most for Capriolo Konnov) was the formation of hydrogen peroxide via hydrogen abstraction of isopropanol by the hydroperoxyl radical in (R2).

$$iC_3H_7OH + HO_2 \rightleftharpoons tC_3H_6OH + H_2O_2 \tag{R2}$$
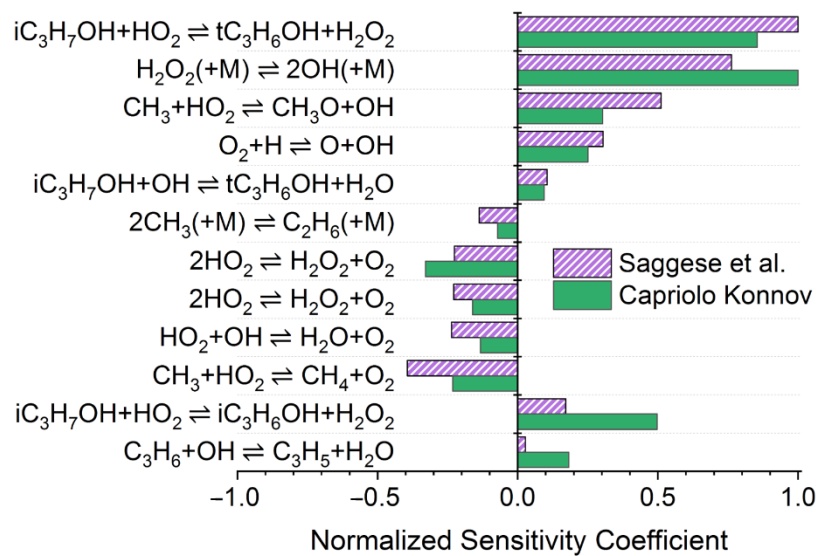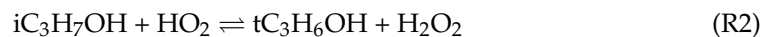
Figure 9. Sensitivity analysis for τ_{ign} using the Capriolo and Konnov and Saggese et al. models conducted at 1100 K, 25 atm, and $\varphi = 0.5$.

Here, tC_3H_6OH is best defined by $(CH_3)_2COH$, meaning, hydrogen is abstracted from the β position of isopropanol in (R2). Interestingly, this result is analogous to the real fuel–air ignition delay time sensitivity of ethanol according to AramcoMech 3.0 [22].

Secondary to Saggese et al. but primary to the Capriolo and Konnov sensitivity was (R3).

$$H_2O_2(+M) \rightleftharpoons 2OH(+M) \tag{R3}$$

This behavior is a natural progression from (R2) (where hydrogen peroxide is formed) to (R3) where hydrogen peroxide is broken down to add to the hydroxyl radical pool. Tertiary to the Capriolo and Konnov model was (R4).

$$iC_3H_7OH + HO_2 \rightleftharpoons iC_3H_6OH + H_2O_2 \tag{R4}$$
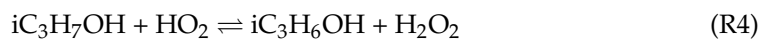
Similar to (R2) where hydrogen peroxide is formed via hydrogen abstraction, here hydrogen is abstracted from the α position (either side since isopropanol is symmetric) to form $CH_2(CHOH)CH_3$ (iC_3H_6OH in the Saggese et al. kinetics mechanism). This step is intuitive since Capriolo and Konnov suggested (R3) as the most important reaction due to the production of hydrogen peroxide from two major sources. Due to this difference, the Saggese et al. model increased the hydroxyl radical pool by suggesting (R5) as having similar sensitivity to (R3).

$$CH_3 + HO_2 \rightleftharpoons CH_3O + OH \tag{R5}$$
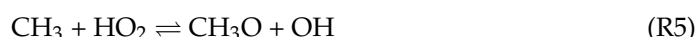
This route also leads to a bottle-necking of hydroperoxyl radical production in the Saggese et al. model due to methane oxidation via (R6).

$$CH_3 + HO_2 \rightleftharpoons CH_4 + O_2 \tag{R6}$$

Note, both kinetics mechanisms included two separate reaction rates for (R7/8).

$$2HO_2 \rightleftharpoons H_2O_2 + O_2 \tag{R7/8}$$

Both mechanisms showed τ_{ign} as being sensitive to (R7/8). This specification of two rates is due to the changing temperature during ignition, requiring the use of two different reaction rates during the temperature increase due to combustion. Figure 9 lists (R7) and (R8) in the order they appear in both mechanisms.

4. Discussion

Using the new reaction rate measured by Cooper et al. for (R1), the Li et al. model was modified to examine the improvements the new reaction rate had on the model prediction for the oxidation experiments [21]. A comparison between the two predictions of the modified and unmodified Li et al. models is shown in Figure 10. Figure 10a,b shows water time histories for high- and low-temperature conditions, where a small improvement from the new reaction rate was seen. Particularly for the high-temperature case, the model was under reactive for the initial water production before 250 μs and over reactive for the secondary water production at longer times. Using the new rate, both the over-reactivity and under-reactivity of the model were reduced. Additionally, CO time histories were taken for these same experiments, and Figure 10c,d shows the CO profiles at the same conditions as Figure 10a,d, respectively. Again, only a small improvement was seen; however, opposed to the water results, Li et al. was over-reactive throughout the experiment. The new rate reduced the reactivity of the model for these profiles and in fact more significantly improved CO predictions than it did for water.

Previous studies have established the need for helium addition to mixtures to hasten CO vibrational relaxation for combustion in methane mixtures [42,53]. These experiments, conducted in methane, showed significant improvement in model prediction with the addition of helium. It was explained that some CO is formed in an excited vibrational state, and helium hastened the relaxation of these molecules to the ground state. However, helium is also a more efficient collision partner than argon, and the experiments were conducted below the high-pressure limit for methane combustion. That is, experiments conducted with a more-efficient collider would more closely match the model predictions for the same conditions as those without the helium addition. Reactions for isopropanol at these pressures (near atmospheric), however, have been shown to be within the high-pressure limit [21]. With this in mind, experiments were conducted without helium as a

diluent for conditions similar to those with helium. A comparison of two experimental CO time histories for mixtures with and without helium around 1460 K is shown in Figure 11.
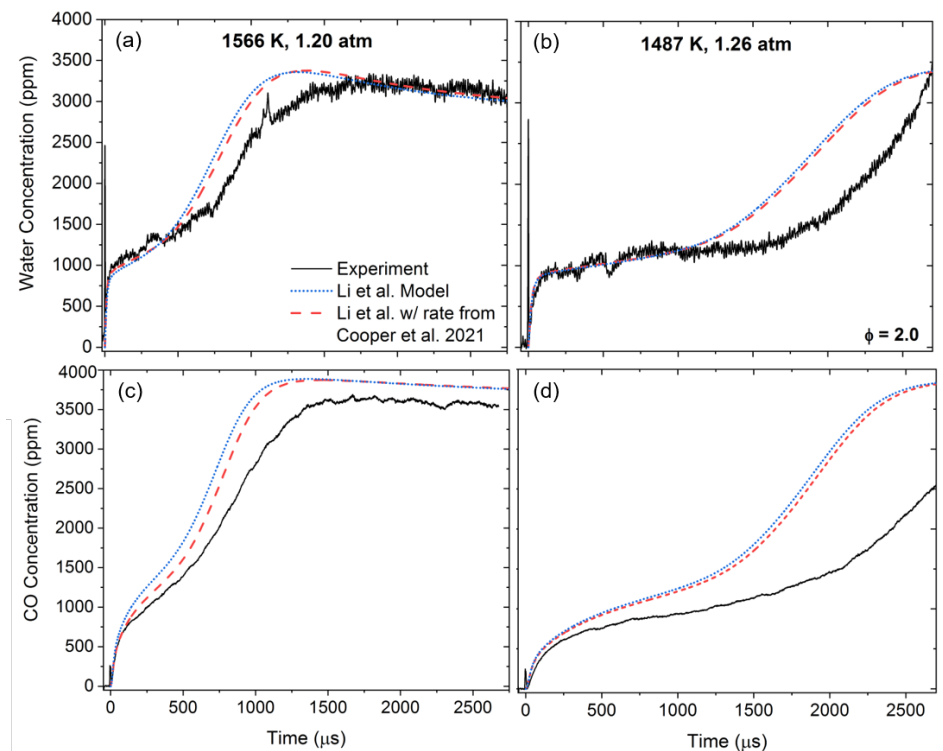

Figure 10. Comparison of predictions made by the Li et al. model and those made by the Li et al. model using the reaction rate presented by Cooper et al. [21] for (R1). Profiles (**a**,**c**) were taken simultaneously in an experiment at 1566 K and 1.20 atm, and (**b**,**d**) were taken at 1487 K and 1.26 atm. Both experiments were conducted with the $\varphi = 2.0$ mixture.
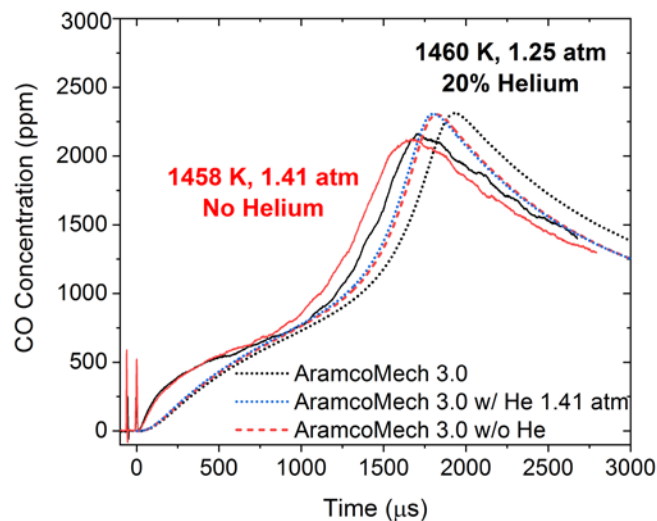
Figure 11. Effect of helium addition on CO production and model predictions for stoichiometric oxidation of isopropanol at ~1460 K. The AramcoMech 3.0 mechanism predictions for the two runs are also shown to investigate the effect of test pressure.

In the previous studies in methane, the addition of helium shortened the induction time for CO production, which would be expected with a more efficient collision partner [42]. However, the addition of helium in mixtures studied herein showed the opposite effect at longer times. Meaning, for the secondary increase of CO during isopropanol

oxidation, the mixture without helium was artificially faster. However, this trend was not seen for the initial CO formation, where the most sensitive reactions for isopropanol were within the high-pressure limit. Note, due to the reduced shock efficiency of helium in the driven section, the test pressure of the resulting experiment was reduced for the mixtures with helium. Therefore, predictions by AramcoMech 3.0 are also shown in Figure 11. Note, the AramcoMech 3.0 model was state independent. While the model predicted slower CO production curves, the time shift due to the increased pressure in the experiment without helium was nearly identical to the one seen in the experiment. Additionally, the AramcoMech 3.0 model was run using the mixture containing helium at the increased pressure (1.41 atm instead of 1.25 atm) at 1460 K and is also shown in Figure 11. Here, the profiles with and without helium at the same pressure were virtually the same. Meaning, the difference was predicted to be mainly due to the pressure difference. Therefore, for isopropanol combustion, the effect of helium addition, in terms of accelerating vibrational relaxation, had little influence on the production of CO.

A regression analysis was performed using the 10- and 25-atm ignition delay time data presented herein to quantify isopropanol's dependence on equivalence ratio, pressure, and temperature. This analysis yielded Equation (1):

$$\tau_{ign} = 0.022 \varphi^{-0.527} P^{-0.947} e^{\frac{27.7}{RT}} \tag{1}$$

Equation (1) has an R^2 value of 0.988 and a standard error of 12.4%, suggesting a great representation of the data. A comparison of the predicted values and the measured values are supplied in the Supplemental Material. Equation (1) highlights some of the characteristics shown in Figure 8. Particularly, what was seen is a dependency on the pressure that was about twice that of the equivalence ratio. Interestingly, the pressure, equivalence ratio, and temperature dependencies shown for isopropanol were remarkably similar to those found previously for gasoline surrogates, suggesting comparable 0-D ignition behavior [39]. Although spark-ignition engines typically operate at higher pressures and with undiluted fuel–air mixtures, these findings aid modeling efforts for such engines, specifically with regard to tuning the chemical kinetics of isopropanol at high temperatures.

5. Conclusions

New data for isopropanol oxidation and pyrolysis are presented. Pyrolysis and oxidation experiments (for $\varphi = 0.5$, 1.0, and 2.0) were conducted under highly dilute conditions to measure CO and water production using laser absorption at near-atmospheric pressures. Four modern chemical kinetics models for isopropanol combustion were investigated. The Li et al. and Saggese et al. models were both found to have the best ability to predict CO and water production under pyrolysis conditions, while the AramcoMech 3.0 and Capriolo and Konnov models were seen to better predict the oxidation experimental profiles. Ignition delay time experiments were also conducted under real fuel–air conditions for isopropanol at 10 and 25 atm and for $\varphi = 0.5$ and 1.0, wherein discrepancies with previous experiments were seen for 10-atm results. These discrepancies were shown to be due to improper usage of sidewall diagnostics to define ignition during real fuel–air experiments in shock tubes. It was found that the AramcoMech 3.0 model over predicted τ_{ign} values, while the Li et al. model severely under predicted τ_{ign}. The models by Capriolo and Konnov and Saggese et al. were found to be in good agreement with experimental τ_{ign} values, and they were thus used to conduct a sensitivity analysis to highlight the underlying chemistry at 25 atm. Additionally, the Li et al. model was modified using a recently measured reaction rate, and some slight improvement in the model's predictions of CO and water profiles during dilute oxidation was shown. Finally, a regression analysis was performed to quantify τ_{ign} results from this study.

References

1. Agarwal, A.K.; Kim, J. Biofuels (alcohols and biodiesel) applications as fuels for internal combustion engines. *Prog. Energy Combust. Sci.* **2007**, *33*, 233–271. [CrossRef]
2. Co-Optima. Available online: https://energy.gov/eere/bioenergy/co-optimization-fuels-engines (accessed on 21 January 2019).
3. McCormick, R.; Fioroni, G.; Fouts, L.; Christensen, E.; Yanowitz, J.; Polikarpov, E.; Albrecht, K.; Gaspar, D.; Gladden, J.; George, A. Selection Criteria and Screening of Potential Biomass-Derived Streams as Fuel Blendstocks for Advanced Spark-Ignition Engines. *SAE Int. J. Fuels Lubr.* **2017**, *10*, 442–460. [CrossRef]
4. Gaspar, D.J.; West, B.H.; Ruddy, D.; Wilke, T.J.; Polikarpov, E.; Alleman, T.L.; George, A.; Monroe, E.; Davis, R.W.; Vardon, D.; et al. *Top Ten Blendstocks Derived from Biomass for Turbocharged Spark Ignition Engines: Bio-Blendstocks with Potential for Highest Engine Efficiency*; Pacific Northwest National Lab (PNNL): Richland, WA, USA, 2019.
5. Mathieu, O.; Sikes, T.; Kulatilaka, W.D.; Petersen, E.L. Ignition delay time and laminar flame speed measurements of mixtures containing diisopropyl-methylphosphonate (DIMP). *Combust. Flame* **2020**, *215*, 66–77. [CrossRef]
6. Fuller, M.E.; Goldsmith, C.F. Shock Tube Laser Schlieren Study of the Pyrolysis of Isopropyl Nitrate. *J. Phys. Chem. A* **2019**, *123*, 5866–5876. [CrossRef] [PubMed]
7. Smith, S.R.; Gordon, A.S. Studies of Diffusion Flames. II. Diffusion Flames of Some Simple Alcohols. *J. Phys. Chem.* **1956**, *60*, 1059–1062. [CrossRef]
8. Norton, T.S.; Dryer, F.L. The flow reactor oxidation of C1−C4 alcohols and MTBE. *Proc. Combust. Inst.* **1991**, *23*, 179–185. [CrossRef]
9. Sinha, A.; Thomson, M. The chemical structures of opposed flow diffusion flames of C3 oxygenated hydrocarbons (isopropanol, dimethoxy methane, and dimethyl carbonate) and their mixtures. *Combust. Flame* **2004**, *136*, 548–556. [CrossRef]
10. Frassoldati, A.; Cuoci, A.; Faravelli, T.; Niemann, U.; Ranzi, E.; Seiser, R.; Seshadri, K. An experimental and kinetic modeling study of n-propanol and iso-propanol combustion. *Combust. Flame* **2010**, *157*, 2–16. [CrossRef]
11. Esarte, C.; Abián, M.; Millera, Á.; Bilbao, R.; Alzueta, M.U. Gas and soot products formed in the pyrolysis of acetylene mixed with methanol, ethanol, isopropanol or n-butanol. *Energy* **2012**, *43*, 37–46. [CrossRef]
12. Li, W.; Zhang, Y.; Mei, B.; Li, Y.; Cao, C.; Zou, J.; Yang, J.; Cheng, Z. Experimental and kinetic modeling study of n-propanol and i-propanol combustion: Flow reactor pyrolysis and laminar flame propagation. *Combust. Flame* **2019**, *207*, 171–185. [CrossRef]
13. Li, Y.; Wei, L.; Tian, Z.; Yang, B.; Wang, J.; Zhang, T.; Qi, F. A comprehensive experimental study of low-pressure premixed C3-oxygenated hydrocarbon flames with tunable synchrotron photoionization. *Combust. Flame* **2008**, *152*, 336–359. [CrossRef]
14. Kasper, T.; Oßwald, P.; Struckmeier, U.; Kohse-Höinghaus, K.; Taatjes, C.; Wang, J.; Cool, T.; Law, M.; Morel, A.; Westmoreland, P. Combustion chemistry of the propanol isomers—Investigated by electron ionization and VUV-photoionization molecular-beam mass spectrometry. *Combust. Flame* **2009**, *156*, 1181–1201. [CrossRef]
15. Togbé, C.; Dagaut, P.; Halter, F.; Foucher, F. 2-Propanol Oxidation in a Pressurized Jet-Stirred Reactor (JSR) and Combustion Bomb: Experimental and Detailed Kinetic Modeling Study. *Energy Fuels* **2011**, *25*, 676–683. [CrossRef]
16. Johnson, M.V.; Goldsborough, S.S.; Serinyel, Z.; O'Toole, P.; Larkin, E.; O'Malley, G.; Curran, H.J. A shock tube study of n-and iso-propanol ignition. *Energy Fuels* **2009**, *23*, 5886–5898. [CrossRef]
17. Akih-Kumgeh, B.; Bergthorson, J.M. Ignition of C3 oxygenated hydrocarbons and chemical kinetic modeling of propanal oxidation. *Combust. Flame* **2011**, *158*, 1877–1889. [CrossRef]

18. Man, X.; Tang, C.; Zhang, J.; Zhang, Y.; Pan, L.; Huang, Z.; Law, C.K. An experimental and kinetic modeling study of n-propanol and i-propanol ignition at high temperatures. *Combust. Flame* **2014**, *161*, 644–656. [CrossRef]

19. Jouzdani, S.; Zhou, A.; Akih-Kumgeh, B. Propanol isomers: Investigation of ignition and pyrolysis time scales. *Combust. Flame* **2017**, *176*, 229–244. [CrossRef]

20. Cheng, S.; Kang, D.; Goldsborough, S.S.; Saggese, C.; Wagnon, S.W.; Pitz, W.J. Experimental and modeling study of C2–C4 alcohol autoignition at intermediate temperature conditions. *Proc. Combust. Inst.* **2021**, *38*, 709–717. [CrossRef]

21. Cooper, S.P.; Mulvihill, C.R.; Mathieu, O.; Petersen, E.L. Isopropanol dehydration reaction rate kinetics measurement using H_2O time histories. *Int. J. Chem. Kinet.* **2021**, *53*, 536–547. [CrossRef]

22. Mathieu, O.; Pinzón, L.T.; Atherley, T.M.; Mulvihill, C.R.; Schoel, I.; Petersen, E.L. Experimental study of ethanol oxidation behind reflected shock waves: Ignition delay time and H_2O laser-absorption measurements. *Combust. Flame* **2019**, *208*, 313–326. [CrossRef]

23. Pinzón, L.T.; Mathieu, O.; Mulvihill, C.R.; Schoegl, I.; Petersen, E.L. Ethanol pyrolysis kinetics using H2O time history measurements behind reflected shock waves. *Proc. Combust. Inst.* **2019**, *37*, 239–247. [CrossRef]

24. Mertens, L.A.; Manion, J.A. Kinetics of isopropanol decomposition and reaction with H atoms from shock tube experiments and rate constant optimization using the method of uncertainty minimization using polynomial chaos expansions (MUM-PCE). *Int. J. Chem. Kinet.* **2021**, *53*, 95–126. [CrossRef]

25. Veloo, P.S.; Egolfopoulos, F. Studies of n-propanol, iso-propanol, and propane flames. *Combust. Flame* **2011**, *158*, 501–510. [CrossRef]

26. Sarathy, S.M.; Osswald, P.; Hansen, N.; Kohse-Höinghaus, K. Alcohol combustion chemistry. *Prog. Energy Combust. Sci.* **2014**, *44*, 40–102. [CrossRef]

27. Zhou, C.-W.; Li, Y.; Burke, U.; Banyon, C.; Somers, K.P.; Ding, S.; Khan, S.; Hargis, J.W.; Sikes, T.; Mathieu, O.; et al. An experimental and chemical kinetic modeling study of 1,3-butadiene combustion: Ignition delay time and laminar flame speed measurements. *Combust. Flame* **2018**, *197*, 423–438. [CrossRef]

28. Liu, X.; Wang, H.; Zheng, Z.; Liu, J.; Reitz, R.D.; Yao, M. Development of a combined reduced primary reference fuel-alcohols (methanol/ethanol/propanols/butanols/n-pentanol) mechanism for engine applications. *Energy* **2016**, *114*, 542–558. [CrossRef]

29. Capriolo, G.; Konnov, A. Combustion of propanol isomers: Experimental and kinetic modeling study. *Combust. Flame* **2020**, *218*, 189–204. [CrossRef]

30. Saggese, C.; Thomas, C.M.; Wagnon, S.W.; Kukkadapu, G.; Cheng, S.; Kang, D.; Goldsborough, S.S.; Pitz, W.J. An improved detailed chemical kinetic model for C3-C4 linear and iso-alcohols and their blends with gasoline at engine-relevant conditions. *Proc. Combust. Inst.* **2021**, *38*, 415–423. [CrossRef]

31. Petersen, E.; Rickard, M.J.A.; Crofton, M.W.; Abbey, E.D.; Traum, M.J.; Kalitan, D.M. A facility for gas- and condensed-phase measurements behind shock waves. *Meas. Sci. Technol.* **2005**, *16*, 1716–1729. [CrossRef]

32. Lipkowicz, J.T.; Nativel, D.; Cooper, S.; Wlokas, I.; Fikri, M.; Petersen, E.; Schulz, C.; Kempf, A.M. Numerical Investigation of Remote Ignition in Shock Tubes. *Flow, Turbul. Combust.* **2021**, *106*, 471–498. [CrossRef]

33. Mulvihill, C.R.; Alturaifi, S.A.; Petersen, E.L. A shock-tube study of the $N_2O + M \rightleftarrows N_2 + O + M$ (M = Ar) rate constant using N_2O laser absorption near 4.6 μm. *Combust. Flame* **2021**, *224*, 6–13. [CrossRef]

34. Vivanco, J.E. A New Shock-Tube Facility for the Study of High-Temperature Chemical Kinetics. Master's Thesis, Texas A&M University, College Station, TX, USA, 2014.

35. Zander, L.; Vinkeloe, J.; Djordjevic, N. Ignition delay and chemical–kinetic modeling of undiluted mixtures in a high-pressure shock tube: Nonideal effects and comparative uncertainty analysis. *Int. J. Chem. Kinet.* **2021**, *53*, 611–637. [CrossRef]

36. Hargis, J.W.; Petersen, E.L. Shock-Tube Boundary-Layer Effects on Reflected-Shock Conditions with and without CO_2. *AIAA J.* **2017**, *55*, 902–912. [CrossRef]

37. Nativel, D.; Cooper, S.P.; Lipkowicz, T.; Fikri, M.; Petersen, E.L.; Schulz, C. Impact of shock-tube facility-dependent effects on incident- and reflected-shock conditions over a wide range of pressures and Mach numbers. *Combust. Flame* **2020**, *217*, 200–211. [CrossRef]

38. Alturaifi, S.A.; Rebagay, R.L.; Mathieu, O.; Guo, B.; Petersen, E.L. A Shock-Tube Autoignition Study of Jet, Rocket, and Diesel Fuels. *Energy Fuels* **2019**, *33*, 2516–2525. [CrossRef]

39. Cooper, S.P.; Mathieu, O.; Schoegl, I.; Petersen, E.L. High-pressure ignition delay time measurements of a four-component gasoline surrogate and its high-level blends with ethanol and methyl acetate. *Fuel* **2020**, *275*, 118016. [CrossRef]

40. Mathieu, O.; Mulvihill, C.; Petersen, E.L. Shock-tube water time-histories and ignition delay time measurements for H2S near atmospheric pressure. *Proc. Combust. Inst.* **2017**, *36*, 4019–4027. [CrossRef]

41. Mulvihill, C.R.; Petersen, E.L. Concerning shock-tube ignition delay times: An experimental investigation of impurities in the H2/O2 system and beyond. *Proc. Combust. Inst.* **2019**, *37*, 259–266. [CrossRef]

42. Mathieu, O.; Mulvihill, C.; Petersen, E.L. Assessment of modern detailed kinetics mechanisms to predict CO formation from methane combustion using shock-tube laser-absorption measurements. *Fuel* **2019**, *236*, 1164–1180. [CrossRef]

43. Mathieu, O.; Cooper, S.; Alturaifi, S.A.; Mulvihill, C.R.; Atherley, T.; Petersen, E.L. Shock-Tube Laser Absorption Measurements of CO and H2O during Iso-Octane Combustion. *Energy Fuels* **2020**, *34*, 7533–7544. [CrossRef]

44. Mulvihill, C.R.; Keesee, C.L.; Sikes, T.; Teixeira, R.S.; Mathieu, O.; Petersen, E.L. Ignition delay times, laminar flame speeds, and species time-histories in the H2S/CH4 system at atmospheric pressure. *Proc. Combust. Inst.* **2019**, *37*, 735–742. [CrossRef]

45. Petersen, E.L. Interpreting Endwall and Sidewall Measurements in Shock-Tube Ignition Studies. *Combust. Sci. Technol.* **2009**, *181*, 1123–1144. [CrossRef]
46. Ansys. *ChemKin 19.1*; Ansys: San Diego, CA, USA, 2018.
47. Pelucchi, M.; Cavallotti, C.; Faravelli, T.; Klippenstein, S.J. H-Abstraction reactions by OH, HO$_2$, O, O$_2$ and benzyl radical addition to O$_2$ and their implications for kinetic modelling of toluene oxidation. *Phys. Chem. Chem. Phys.* **2018**, *20*, 10607–10627. [CrossRef] [PubMed]
48. Cai, J.; Zhang, L.; Zhang, F.; Wang, Z.; Cheng, Z.; Yuan, W.; Qi, F. Experimental and Kinetic Modeling Study of n-Butanol Pyrolysis and Combustion. *Energy Fuels* **2012**, *26*, 5550–5568. [CrossRef]
49. Jin, H.; Cai, J.; Wang, G.; Wang, Y.; Li, Y.; Yang, J.; Cheng, Z.; Yuan, W.; Qi, F. A comprehensive experimental and kinetic modeling study of tert-butanol combustion. *Combust. Flame* **2016**, *169*, 154–170. [CrossRef]
50. Sarathy, S.M.; Vranckx, S.; Yasunaga, K.; Mehl, M.; Osswald, P.; Metcalfe, W.K.; Westbrook, C.K.; Pitz, W.J.; Kohse-Höinghaus, K.; Fernandes, R.X.; et al. A comprehensive chemical kinetic combustion model for the four butanol isomers. *Combust. Flame* **2012**, *159*, 2028–2055. [CrossRef]
51. Tsang, W.; Walker, J.A.; Manion, J.A. The decomposition of normal hexyl radicals. *Proc. Combust. Inst.* **2007**, *31*, 141–148. [CrossRef]
52. Heyne, J.S.; Dooley, S.; Serinyel, Z.; Dryer, F.L.; Curran, H. Decomposition Studies of Isopropanol in a Variable Pressure Flow Reactor. *Zeitschrift für Physikalische Chemie* **2015**, *229*, 881–907. [CrossRef]
53. Sen, F.; Shu, B.; Kasper, T.; Herzler, J.; Welz, O.; Fikri, M.; Atakan, B.; Schulz, C. Shock-tube and plug-flow reactor study of the oxidation of fuel-rich CH$_4$/O$_2$ mixtures enhanced with additives. *Combust. Flame* **2016**, *169*, 307–320. [CrossRef]